Journal of Materials Chemistry C

Materials for optical and electronic devices

www.rsc.org/MaterialsC

Volume 1 | Number 17 | 7 May 2013 | Pages 2945–3044

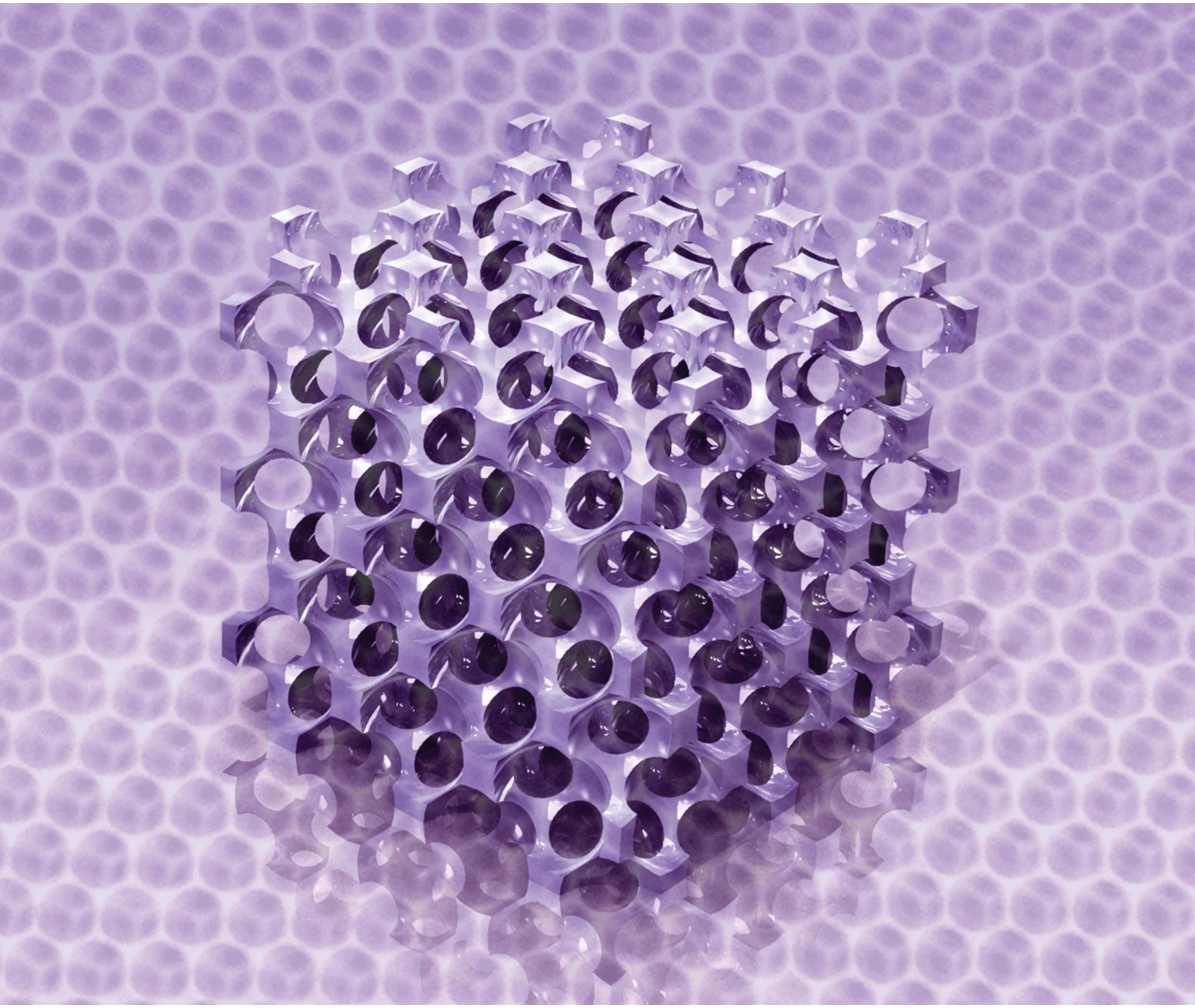

ISSN 2050-7526

RSC Publishing

PAPER

Alexander Sinitskii *et al.*

Synthesis of high-quality inverse opals based on magnetic complex oxides: yttrium iron garnet ($Y_3Fe_5O_{12}$) and bismuth ferrite ($BiFeO_3$)

2050-7526(2013)1:17;1-F

Journal of Materials Chemistry C

RSC Publishing

PAPER

View Article Online
View Journal | View Issue

Cite this: J. Mater. Chem. C, 2013, 1, 2975

Synthesis of high-quality inverse opals based on magnetic complex oxides: yttrium iron garnet ($Y_3Fe_5O_{12}$) and bismuth ferrite ($BiFeO_3$)

Vera V. Abramova,†[a] Alexander Slesarev†[a] and Alexander Sinitskii*[b]

Magnetophotonic crystals (MPCs) are periodic structures that are made of a magnetic material or have a magnetic defect introduced in a periodic non-magnetic matrix, and possess interesting optical and magneto-optical properties. Of particular interest are three-dimensional (3D) MPCs made of magnetic complex oxides, such as yttrium iron garnet ($Y_3Fe_5O_{12}$, YIG) and bismuth ferrite ($BiFeO_3$, BFO). In this paper we report for the first time the synthesis of 3D MPCs with a face-centered cubic (fcc) inverse opal structure based on these materials. The samples were prepared by a sol–gel method that involves infiltration of polystyrene colloidal crystals with liquid precursors followed by a high-temperature annealing. The developed procedure yields high-quality single-phase YIG and BFO inverse opals with high filling fractions of magnetic materials. Optical measurements were performed on large (characteristic size $\sim$ 100 μm) single crystal domains of inverse opals, and angle-dependent reflectance peaks caused by the Bragg diffraction of light in highly ordered YIG and BFO MPCs were observed. Also, since BFO has a high refractive index (>2.8) and a low extinction coefficient at λ > 550 nm, BFO MPCs with the fcc structure have a potential for the realization of a complete photonic band gap in the visible and near infrared regions.

Received 21st February 2013
Accepted 11th March 2013

DOI: 10.1039/c3tc30335g

www.rsc.org/MaterialsC

1 Introduction

Photonic crystals (PCs) are periodic microstructures that could be used to manipulate the flow of light.[1] Of particular interest are so-called magnetophotonic crystals (MPCs) that are made of a magnetic material or have a magnetic defect introduced in a periodic non-magnetic matrix, and possess interesting optical and magneto-optical properties.[2] So far, most of the experimental studies of MPCs focused on one-dimensional (1D) structures, which could be fabricated by consecutive deposition of magnetic and nonmagnetic layers.[2] If a magnetic microcavity is introduced in a periodic layered structure, localization of light in the magnetic defect results in a significant enhancement of Faraday and Kerr rotations,[3,4] and nonlinear magneto-optical Kerr effect (NOMOKE) or magnetization-induced variations in second harmonic generation (MSHG) intensity.[5–7] Similarly, light localization on a planar defect introduced in a colloidal crystal[8] results in enhancement of Faraday effect. In case of completely periodic 1D MPCs without microcavities enhanced NOMOKE and Faraday effects were observed near a photonic band edge.[9]

Two- and three-dimensional (2D and 3D) MPCs are expected to exhibit not only all effects predicted and observed for 1D MPCs, but also several additional theoretically predicted phenomena, such as strong spectral asymmetry,[10] Faraday band effect,[11] tunable refraction phenomena,[12] and others. However, experimental verification of these theories requires fabrication of high-quality 2D or 3D MPCs, which remains very challenging.

A possible route toward high-quality 3D MPCs involves infiltration of colloidal crystals based on monodisperse silica or polymer spheres with magnetic materials followed by removal of colloidal spheres.[1,13] This templating approach was shown to be very versatile, allowing fabrication of 3D periodic porous structures, referred to as inverse opals, based on metals, semiconductors, oxides, and polymers.[1,13] However, experimental studies that focused on the preparation of magnetic inverse opals are very limited. Inverse opals could be fabricated by electrodeposition of magnetic metals, such as Fe,[14] Co[14,15] and Ni[14,16–18] in the voids of colloidal crystals. However, due to the non-transparency of metals only surface magneto-optical effects could be probed for such samples.[18,19] In other studies, PCs with magnetic properties were prepared by filling the voids in silica colloidal crystals with magnetite (Fe_3O_4)[20–22] and yttrium iron garnet ($Y_3Fe_5O_{12}$, YIG)[21,23] nanoparticles, but the filling fractions

[a]Department of Materials Science, M. V. Lomonosov Moscow State University, Leninskie Gory, 119991 Moscow, Russia

[b]Department of Chemistry and Nebraska Center for Materials and Nanoscience, University of Nebraska – Lincoln, Lincoln, NE 68588-0304, USA. E-mail: sinitskii@unl.edu; Fax: +1-402-472-9402; Tel: +1-402-617-3543

† Present address: Department of Chemistry, Rice University, Houston, TX 77005, USA.

were typically low; no inverse structures fully made of the above magnetic oxides have been reported so far.

Since YIG and bismuth ferrite ($BiFeO_3$, BFO) are among the most promising materials for 3D MPCs, a development of synthetic approaches for high-quality YIG and BFO inverse opals is of great interest. Unlike many other magnetic materials, YIG is transparent in the infrared region, and exhibits strong magneto-optical and non-linear response.[24–26] Because of its unique properties, YIG and related materials, such as Bi:YIG, were often used for 1D and defect-mode MPCs.[4–9] BFO is also optically transparent in the near infrared region,[27] and also exhibits second harmonic generation and MSHG.[27–29] Furthermore, BFO has recently attracted a lot of attention as a multiferroic material with correlated antiferromagnetic and ferroelectric ordering,[30] in which magnetic switching could be performed by application of an electric field.

Preparation of single-phase complex oxide materials is often difficult, and requires following precise synthetic protocols. For instance, co-precipitation of yttrium and iron hydroxides at the molar ratio Y : Fe = 3 : 5, followed by annealing may result in a mixture of different products, which may include YIG, $YFeO_3$, Y_2O_3, α-Fe_2O_3, where the presence and relative amounts of these phases depend on homogenization of a precursor mixture, annealing temperature and heating rate.[31] Also, high-temperature annealing, which is often involved in specific synthetic protocols for complex oxide materials, may be accompanied by thermal decomposition of precursors, re-crystallization of intermediate and final products, and thermal expansion of a material and a substrate, and therefore could result in the destruction of highly ordered structure of a ceramic inverse opal.[32,33] Therefore, in order to synthesize YIG and BFO inverse opals it is important to find a proper fabrication approach and synthetic conditions that result in single-phase materials without disrupting a periodic structure of 3D MPCs.

In this paper we report for the first time the synthesis of high-quality single-phase BFO and YIG inverse opals with high filling fractions of magnetic materials.

2 Experimental

All reagents were purchased from Aldrich and used as received. Monodisperse polystyrene microspheres were synthesized by the emulsifier-free emulsion polymerization of styrene using potassium persulfate as initiator.[34] We synthesized two batches of spheres with average diameters of 800 and 950 nm, respectively. According to the results of scanning electron microscopy (SEM), in both batches spheres had a narrow size distribution with a relative standard deviation less than 2% (at least 200 spheres were sized in SEM images of each sample).

Spheres were self-assembled on glass substrates by the vertical deposition technique.[35,36] In a typical process, thoroughly cleaned glass substrates were immersed in ~0.5 wt% dispersion of microspheres in water, and kept undisturbed at 50 ± 1 °C until the end of the growth process. Standard microscope slides served as substrates for colloidal crystals that were later used for the synthesis of BFO inverse opals. However, such glass substrates could not be used for the synthesis of YIG inverse opals where the final annealing was performed at 750 °C. Colloidal crystals that were used for the synthesis of YIG inverse opals were grown on heat-resistant glass substrates received from FSUE Technologiya (Obninsk, Russia).

YIG and BFO inverse opals were synthesized by a sol–gel approach based on a modified Pechini method.[37] The experimental conditions for both types of inverse opals are summarized in Table 1. Liquid precursors were prepared by dissolving a certain amount of citric acid in ethanol solution and then adding a stoichiometric mixture of aqueous solutions of the corresponding metal nitrates while stirring (Table 1). The exact concentrations of solutions of metal nitrates were pre-determined by the gravimetrical analysis; $Fe(NO_3)_3$ and $Bi(NO_3)_3$ solutions were acidified to pH ≈ 1 by the addition of a concentrated nitric acid.

For most experiments we used colloidal crystal films consisting of polystyrene microspheres with an average diameter of 800 nm. Colloidal crystal films were dipped in a corresponding precursor solution (Table 1), and the voids between colloidal spheres were filled with a solution by capillary action. Then, the samples were kept for 30 min at 50 °C to form a precursor resin in the voids. Infiltration of colloidal crystals with BFO or YIG precursors was performed 2–3 times. Finally, the samples were annealed in air to form corresponding complex oxides and remove polystyrene spheres; the annealing procedures for both YIG and BFO are presented in Table 1.

Thermogravimetrical analysis (TGA) was performed using a Perkin Elmer Pyris Diamond instrument. Phase composition of the samples was studied by powder X-ray diffraction (XRD) analysis using a Rigaku D/MAX 2500 diffractometer with a filtered CuKα radiation. SEM images of the samples were recorded using a Leo Supra 50VP microscope in a variable pressure mode with the acceleration voltage of 15 keV. Prior to imaging, the samples were not coated with any conductive material enabling further optical studies.

Optical measurements were performed using a home-built spectrometer setup with a tungsten lamp as a light source. The light beam was focused on a sample using a pinhole and lens system, so that the probed area of a sample had a diameter of ~100 μm, and the angular aperture of the incident beam was less than 1°. Optical reflectance spectra were recorded in the Bragg geometry in a wide range of incident angles (5–58°) with a focusing lens system and a waveguide connected to a CCD camera. An optical microscope was incorporated in this setup to ensure that angle-dependent reflectance spectra were recorded on the same domain of an inverse opal, and the domain was properly aligned relative to the incident and reflected beams.

3 Results and discussion

Vertical deposition is a self-assembly technique that is often used for the growth of high-quality colloidal crystal films.[35,36,38] A typical film consists of regions with nearly perfect face-centered cubic (fcc) structure, in which close-packed layers of colloidal spheres are parallel to a substrate.[39,40] These regions form domains separated by small cracks that appear during the drying of a colloidal crystal. A film thickness[35] and an average domain size[41] both depend on the concentration of colloidal

spheres in a growth solution. Colloidal crystal films grown in this work were 25–30 layers thick, and consisted of domains with a characteristic size over 200 μm.

Pechini method is often used for the low cost sol–gel synthesis of complex oxides.[37] In the method, a material is synthesized by thermal decomposition of an intermediate resin compound prepared using a complexing agent (typically, citric acid). The resin compound ensures a very uniform mixing of metal ions, which results in significant decrease in annealing temperature compared to other methods for ceramic synthesis. Previously, Pechini method and its modifications were demonstrated to facilitate the synthesis of BFO[42,43] and YIG[44] powders.

Table 1 Synthetic conditions for YIG and BFO inverse opals

Composition	Precursors	Annealing
$BiFeO_3$	0.46 M $Fe(NO_3)_3$, 0.46 M $Bi(NO_3)_3$, 0.92 M citric acid. *Solvent*: water–ethanol (1 : 1)	Slow heating (0.5 °C min^{-1}) from room temperature (RT) to 500 °C followed by annealing for 1 h.
$Y_3Fe_5O_{12}$	0.92 M $Fe(NO_3)_3$, 0.55 M $Y(NO_3)_3$, 1.47 M citric acid. *Solvent*: water–ethanol (1 : 1)	*Step 1*: slow heating (0.5 °C min^{-1}) from RT to 400 °C followed by annealing for 1 h. *Step 2*: fast introduction in a furnace at 750 °C; annealing for 1 h.

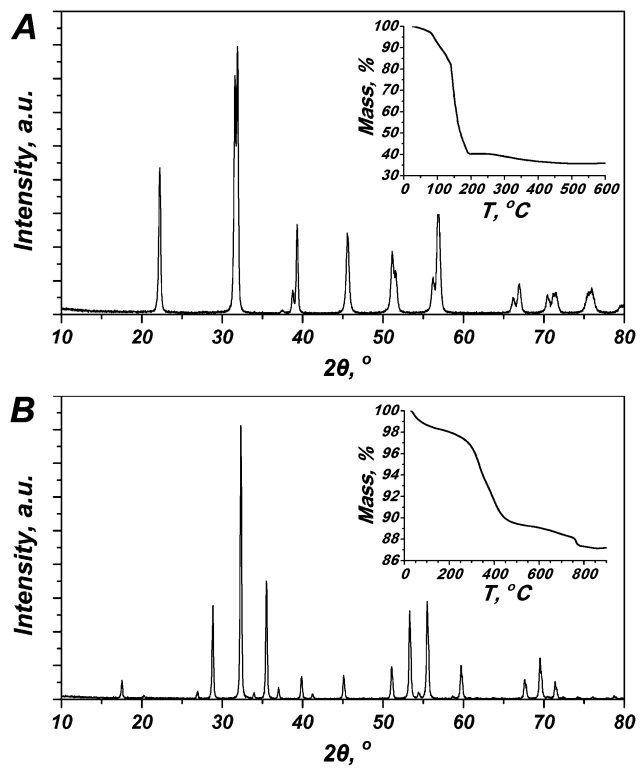

Fig. 1 X-ray powder diffraction results for (A) bismuth ferrite and (B) yttrium-iron garnet. Insets present thermogravimetric analysis results for corresponding resin precursors.

Resin samples prepared from precursor solutions (Table 1) were studied by TGA. The mass losses were recorded while the samples were heated up to 900 °C at the heating rate of 10 °C min^{-1}. During the annealing of a BFO precursor resin the mass loss ends at *ca.* 450–500 °C (see the inset in Fig. 1A). In case of the YIG synthesis, the most significant mass loss occurs in a temperature range between 300 and 400 °C, and then another mass loss step is observed at about 750 °C (see the inset in Fig. 1B). It is also known that the complete decomposition of polystyrene microspheres occurs at *ca.* 300 °C.[33,45] These TGA results were used to select optimal annealing regimes for YIG and BFO inverse opals, see Table 1. It should be noted that in case of the synthesis of YIG inverse opals it was found to be important to perform a two-step annealing with different heating rates in each step. In the first annealing (400 °C) it is essential to heat a sample slowly to preserve its highly ordered structure inherited from a colloidal crystal. In the second step, the fast introduction of a sample to a furnace pre-heated up to 750 °C is required for the crystallization of single-phase $Y_3Fe_5O_{12}$, because the slow heating of a sample up to 750 °C yields a mixture of $YFeO_3$ and α-Fe_2O_3.

Fig. 1 shows XRD patterns of the BFO and YIG powders prepared by annealing precursor resins using the conditions specified in Table 1. In both cases, single phase products ($BiFeO_3$ and $Y_3Fe_5O_{12}$, respectively) are observed. XRD patterns recorded directly from BFO and YIG inverse opals also correspond to single phase materials, and the only difference observed is the presence of a broad halo peak caused by amorphous glass substrates. As anticipated, particles of YIG inverse opals that occasionally peeled off from the substrates were attracted to a magnet.

Fig. 2 shows SEM images of BFO and YIG inverse opals recorded at different magnifications. Removal of volatile components, such as water, CO_2 and NO_2, during the annealing of a polystyrene–resin composite results in significant shrinkage of a structure and formation of additional defects.[46,47] This shrinkage results in the formation of isolated inverse opal domains with a highly ordered structure; representative SEM images of such domains are shown in panels 2A (BFO) and 2D (YIG). Since the size of these domains cannot exceed the size of domains in starting colloidal crystals, growth of high-quality films of polystyrene spheres is the key requirement to prepare large domains of inverse opals. In our experiments, templating colloidal crystals with a characteristic domain size >200 μm resulted in BFO and YIG inverse opals with domains over 100 × 70 μm^2 in size (Fig. 2A and D), which are large enough for single-domain spectroscopic measurements.[48,49]

Fig. 2E shows a side-view SEM image of a YIG inverse opal domain that consists of *ca.* 30 layers. It demonstrates that the regular arrangement of close-packed layers inherited from a colloidal crystal template was not disturbed during the inverse opal synthesis. Typically, the inverse opal domains, observed in side-view SEM images, were 20–30 layers thick, which is in a good agreement with the thicknesses of the starting colloidal crystal films.

Fig. 2C and F show typical high-magnification SEM images of domains of the inverse opals based on BFO and YIG,

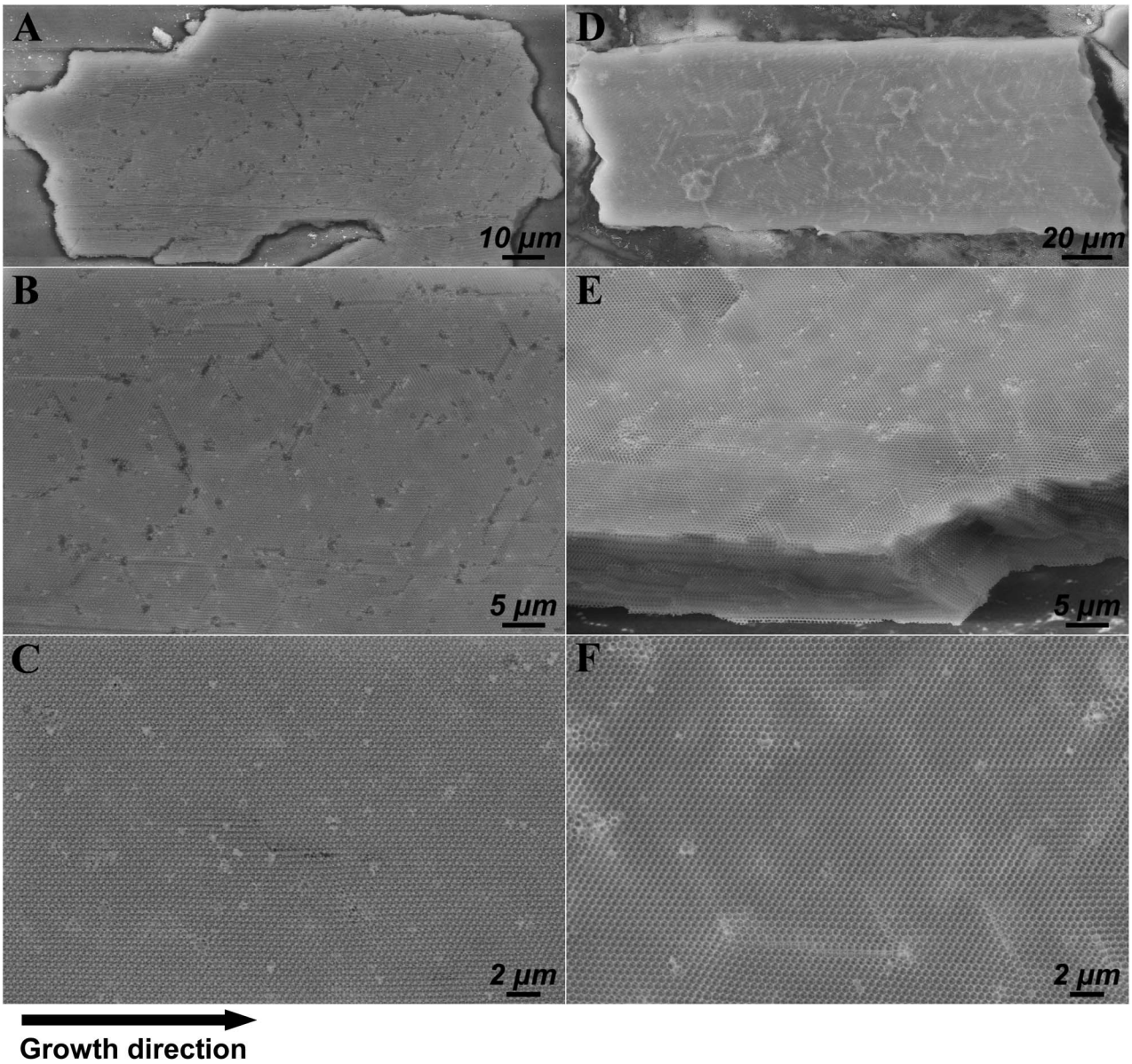

Fig. 2 SEM images of (A–C) BFO and (D–F) YIG inverse opals. All panels show top-view images of the samples except for panel E (side view). In panels A–D and F, growth directions of colloidal crystals used for the synthesis of inverse opals are the same and shown by the black arrow at the bottom of the figure.

respectively. For each sample we have calculated an average distance between the centers of spherical voids in a top hexagonal layer. The values could be slightly different for different domains, but were nearly the same when measured for different areas of the same domain. The average distances vary between 380 and 400 nm for BFO inverse opals, and between 440 and 470 nm for YIG inverse opals – in both cases the values are significantly smaller than the size of starting polystyrene spheres (800 nm). Thus, the in-plane structural shrinkage for the reported synthetic procedure is 50–52% for BFO inverse opals, and 41–44% for YIG inverse opals.

In order to probe intrinsic optical properties of BFO and YIG inverse opals, we have used a single-domain optical spectroscopy to avoid a possible contribution from multiple domains with slightly different structure periodicities, crystallographic orientations and thicknesses. Reflectance spectra were recorded from spots of *ca.* 100 μm in diameter in the wide range of incident angles (θ = 5–58°). Noteworthy, when the incident angles were close to the normal ($\theta = 5°$) similar spectra were recorded for small spots of ~100 μm in diameter, which corresponded to single domains of inverse opals, and much larger areas of 1–2 mm in diameter, which comprised multiple domains. This further confirms that different domains within a single sample had nearly the same periodicities.

The growth of a thick colloidal crystal film by the vertical deposition technique typically occurs along the $[0\bar{2}2]$ crystallographic direction with (111) close-packed layers parallel to the substrate, assuming fcc stacking that is typical for vertically deposited films.[39,40,50] Since the stacking of close-packed layers should not change during the inversion process, we used this

information to ensure a proper crystallographic orientation of inverse opal domains relative to the incident light beam. In the setup used for optical measurements an inverse opal domain was oriented using an optical microscope in a way that the [0$\bar{2}$2] direction was vertical. The incident angle of the light beam was varied in the plane perpendicular to both the [0$\bar{2}\bar{2}$] direction and the substrate. Thus, in terms of the Brillouin zone for the fcc structure the directions scanned were either *LU* or *LK*.

Fig. 3 shows normalized angle-dependent reflectance spectra measured for single domains of BFO and YIG inverse opals, respectively. Let us first consider the spectra recorded close to the normal incidence ($\theta = 5^\circ$). Spectra recorded for both BFO and YIG samples exhibit strong reflection maxima at ~730 and 865 nm, respectively, which correspond to the diffraction of light on (111) planes. The second maximum observed for the BFO inverse opal at ~490 nm (Fig. 3A) most probably corresponds to the diffraction on (222) planes; this maximum is red-shifted if compared to the half of the wavelength position of the (111) maximum, because of a significant increase in BFO refractive index for wavelengths <600 nm.[27] Features observed at $\theta = 5^\circ$ in the spectrum of a YIG inverse opal at the blue edge of the reflectance maximum at ~865 nm (Fig. 3B) could be attributed to Fabry–Pérot oscillations.[35] Inverse opal thickness estimated from the spectral positions of Fabry–Pérot oscillation maxima is 20 layers, which is in a good agreement with the results of SEM.

As the angle of incidence θ increases, the (111) maxima blue-shift (Fig. 3A and B), and the (222) maximum, observed for BFO inverse opal, red-shifts (Fig. 3A). At $\theta = 30^\circ$ another peak close to the (111) maximum becomes noticeable in the spectra recorded for both BFO and YIG inverse opals (Fig. 3); its relative intensity increases with the further increase in the angle of incidence θ, and becomes comparable to the intensity of the (111) maximum at $\theta \sim 40^\circ$. As the angle of incidence θ increases, this peak and the (111) maximum first come closer and then separate again at higher angles, without ever crossing. This behavior was previously observed for both colloidal crystals[39,51] and inverse opals;[52] it was attributed mainly to the band splitting close to *U*(*K*) point of the Brillouin zone. According to Baryshev *et al.*[53] additional peaks in optical reflectance spectra could be explained by the presence of twins in a colloidal crystal structure.

Fig. 4 shows angular dependencies of the positions of diffraction maxima in reflectance spectra shown in Fig. 3. We use λ_{max}^2 *versus* $\sin^2\theta$ coordinates that are typical for the linearization of positions of diffraction maxima in accordance with the Bragg law:

$$\lambda_{max} = 2d\sqrt{n^2 - \sin^2\theta}, \quad (1)$$

where λ_{max} is the spectral position of a diffraction maximum, θ is the angle of incidence, n is the average refractive index of an inverse opal, and d is the interplanar distance. In case of (111) planes $d = (2/3)^{1/2}a$, where a stands for the diameter of a spherical void in the inverse opal structure.

Linearization is correct only for small incident angles,[39,51,52] away from the region where interaction of neighboring zones takes place. Thus, we used only first 4–5 data points for the linearization to estimate the lattice parameters for BFO and YIG inverse opals, and the average refractive indices, which are related to the filling fractions. It should be noted that at high angles of incidence the values corresponding to the second maximum appear to fall on the same line. The average refractive

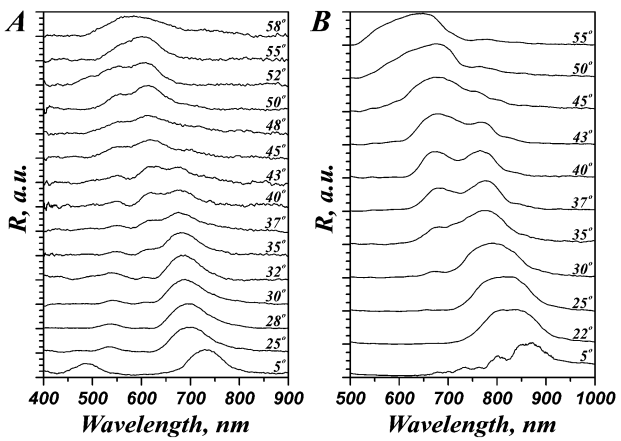

Fig. 3 Normalized angle-dependent optical reflectance spectra recorded for (A) BFO and (B) YIG inverse opals.

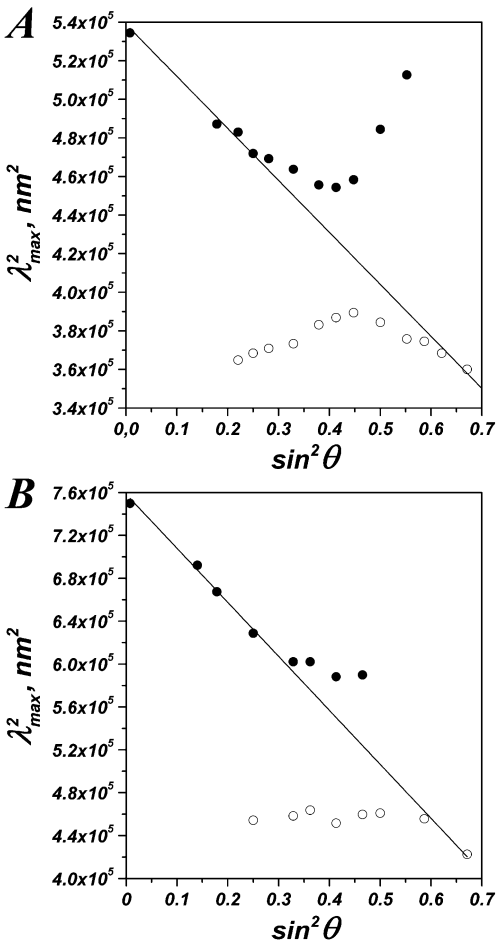

Fig. 4 Linearization of maxima positions observed in reflectance spectra (Fig. 3) for (A) BFO and (B) YIG inverse opals. Black circles show the positions of the first maximum, and white circles show the positions of the second maximum.

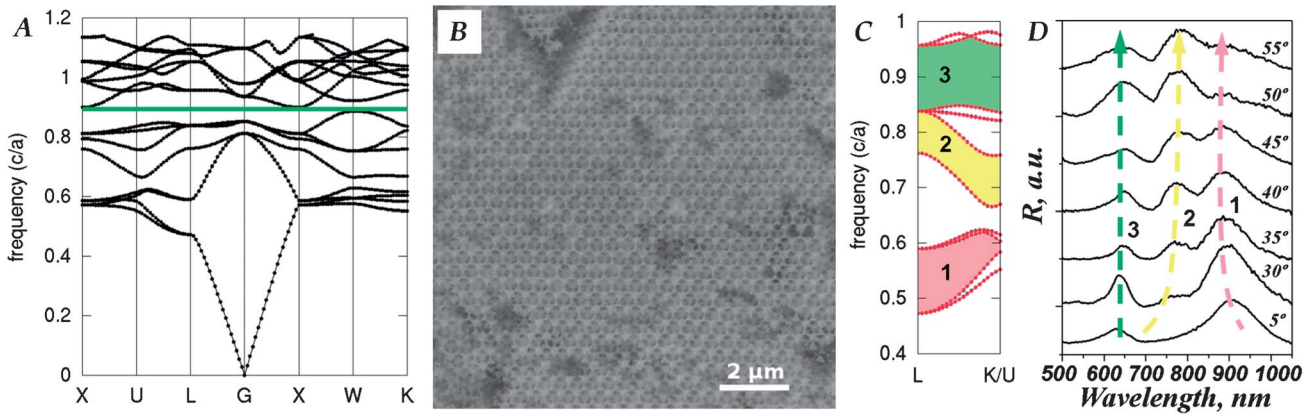

Fig. 5 (A) Band structure for an ideal fcc lattice of air spheres in a material with a refractive index of 3. Green line shows a complete photonic band gap. Frequency is given in c/a units, where c is the speed of light and a is the fcc lattice parameter. (B) SEM image of a BFO inverse opal with a center-to-center distance between spherical voids of ~450 nm. (C) Fragment of a band structure shown in (A) for the L–K/U direction. Colors are used to highlight first (1), second (2) and third (3) photonic band gaps. (D) Normalized angle-dependent optical reflectance spectra recorded for the BFO inverse opal shown in (B). Arrows illustrate the behavior of different reflection peaks; their colors and associated numbers correspond to colors and numbers in (C).

indices estimated from this linearization are 1.41 (BFO inverse opal) and 1.23 (YIG inverse opal), corresponding to the filling fractions of 22% for the BFO inverse opal (assuming that the refractive index of BFO is 2.9 in this wavelength region[27]), and 18% for the YIG inverse opal (assuming that the refractive index of YIG is 2.3 (ref. 26)). Calculated center-to-center distance between spherical voids for the YIG inverse opal is 440 nm, which is in a good agreement with the results of SEM. The value estimated for the BFO inverse opal, 320 nm is slightly smaller than 380–400 nm observed by SEM. This discrepancy could be attributed to either non-uniform shrinkage of the structure during the annealing or non-constancy of the refractive index of BFO[27] in the wavelength region where the linearization was performed.

BFO has a direct electronic band gap of 2.81 eV (442 nm), so it strongly absorbs light in the ultraviolet region, but its extinction coefficient decreases with increasing wavelength, and the material becomes optically transparent at $\lambda > 550$ nm.[27] At those wavelengths, the refractive index of BFO is quite high for optically transparent materials;[1] for instance, at $\lambda = 600$ nm BFO has a refractive index ~3. Interestingly, theoretical calculations suggest that a PC, which has an fcc structure consisting of close-packed spherical voids in a transparent dielectric material, should have a complete photonic band gap if the dielectric material has a refractive index >2.8.[54] Inverse opals based on BFO, which has a refractive index >2.8 and a low extinction coefficient seemingly satisfy this requirement for the visible and near infrared regions. A band structure calculated for an ideal fcc lattice of air spheres in a material with $n = 3$ using the MPB package[55] is shown in Fig. 5A, revealing a complete photonic band gap between the eighth and ninth bands. Considering that the refractive index of BFO is slowly decreasing with increasing wavelength, it would be interesting to study a BFO inverse opal with the gap between the eighth and ninth bands corresponding to $\lambda = 600$ nm, where BFO is optically transparent and has a refractive index above the threshold of 2.8.

We found experimentally that such BFO inverse opals could be synthesized using colloidal crystals of 950 nm polystyrene microspheres as templates, while all other synthetic parameters are kept the same (Table 1). A representative SEM image of one of the samples is shown in Fig. 5B. The average distance between the centers of spherical voids is ~450 nm, which is in correspondence with the linear shrinkage observed for the BFO inverse opals with a smaller structure period. Angle-dependent reflectance spectra corresponding to the path from L to $U(K)$ points of the Brillouin zone were recorded for a single domain of a BFO inverse opal that was aligned as described in the Experimental section. According to the calculated band diagram (Fig. 5C), in the 500–1000 nm range we should observe three photonic gaps. However, in the L point gaps 2 and 3 merge, which explains why at small angles of incidence ($\theta = 5°$) a single broad peak is observed around 630 nm instead of two separate peaks (Fig. 5D). Fig. 5C shows that as the angle of incidence increases, the first photonic band gap should blue-shift, the second one should red-shift, and the third one should stay at nearly the same position. This predicted behavior is observed in Fig. 5D, as illustrated by the arrows. Interestingly, the third peaks in all spectra in Fig. 5D overlap at ~630 nm, suggesting that a complete photonic band gap may be possible in BFO inverse opals with proper lattice parameters. Further experiments focused on the growth of BFO inverse opals of even higher quality and measurements of optical spectra for other critical directions in the Brillouin zone will elucidate whether BFO inverse opals indeed possess a complete photonic band gap.

4 Conclusions

YIG and BFO photonic crystals with the inverse opal structure were prepared by a sol–gel method that involves infiltration of polystyrene colloidal crystals with liquid precursors followed by a high-temperature annealing. According to the SEM and XRD results, the inverse opals had a highly periodic structure and consisted of single-phase YIG and BFO, respectively. The

samples consisted of large (characteristic size ~ 100 μm) single crystal domains of inverse opals, enabling single-domain optical measurements. Spectroscopic measurements revealed angle-dependent reflectance peaks caused by the Bragg diffraction of light in highly ordered YIG and BFO inverse opal domains. These samples are the first examples of 3D MPCs with an inverse opal structure; further studies may result in experimental observation of some of the magneto-optical phenomena theoretically predicted for 3D MPCs. Our results also suggest that BFO inverse opals with proper lattice parameters may possess a complete photonic band gap.

Acknowledgements

The research at Moscow State University was supported by the Russian Foundation for Basic Research (grants ## 07-03-92113 and 08-03-00938) and the Program for Fundamental Research of Russian Academy of Science. The work at UNL was supported by the Nebraska Public Power District through the Nebraska Center for Energy Sciences Research (#12-00-13) and the NSF through Nebraska MRSEC (DMR-0820521) and EPSCoR (EPS-1004094). The authors thank Yu. M. Sofeichuk for the preparation of heat-resistant glass substrates that were used for the synthesis of YIG inverse opals, A. A. Fedyanin for the access to an optical measurement system, M. R. Shcherbakov for assistance with optical measurements, and A. A. Meledin for help with XRD characterization.

Notes and references

1 C. Lopez, *Adv. Mater.*, 2003, **15**, 1679.
2 M. Inoue, R. Fujikawa, A. Baryshev, A. Khanikaev, P. B. Lim, H. Uchida, O. Aktsipetrov, A. Fedyanin, T. Murzina and A. Granovsky, *J. Phys. D: Appl. Phys.*, 2006, **39**, R151.
3 M. Inoue, K. Arai, T. Fujii and M. Abe, *J. Appl. Phys.*, 1999, **85**, 5768.
4 H. Kato, T. Matsushita, A. Takayama, M. Egawa, K. Nishimura and M. Inoue, *J. Magn. Magn. Mater.*, 2004, **272**, E1305.
5 A. A. Fedyanin, T. Yoshida, K. Nishimura, G. Marowsky, M. Inoue and O. A. Aktsipetrov, *JETP Lett.*, 2002, **76**, 527.
6 T. V. Dolgova, A. A. Fedyanin, O. A. Aktsipetrov, K. Nishimura, H. Uchida and M. Inoue, *J. Appl. Phys.*, 2004, **95**, 7330.
7 T. V. Murzina, R. V. Kapra, T. V. Dolgova, A. A. Fedyanin, O. A. Aktsipetrov, K. Nishimura, H. Uchida and M. Inoue, *Phys. Rev. B: Condens. Matter Mater. Phys.*, 2004, **70**, 012407.
8 M. E. Dokukin, A. V. Baryshev, A. B. Khanikaev and M. Inoue, *Opt. Express*, 2009, **17**, 9062.
9 A. A. Fedyanin, O. A. Aktsipetrov, D. Kobayashi, K. Nishimura, H. Uchida and M. Inoue, *J. Magn. Magn. Mater.*, 2004, **282**, 256.
10 A. Figotin and I. Vitebsky, *Phys. Rev. E: Stat., Nonlinear, Soft Matter Phys.*, 2001, **63**, 066609.
11 H. Nishizawa and T. Nakayama, *J. Phys. Soc. Jpn.*, 1997, **66**, 613.
12 A. B. Khanikaev, M. Inoue and A. B. Granovsky, *J. Magn. Magn. Mater.*, 2006, **300**, 104.
13 A. Stein, *Microporous Mesoporous Mater.*, 2001, **44**, 227.
14 P. N. Bartlett, M. A. Ghanem, I. S. El Hallag, P. de Groot and A. Zhukov, *J. Mater. Chem.*, 2003, **13**, 2596.
15 P. N. Bartlett, P. R. Birkin and M. A. Ghanem, *Chem. Commun.*, 2000, 1671.
16 L. B. Xu, W. L. Zhou, M. E. Kozlov, I. I. Khayrullin, I. Udod, A. A. Zakhidov, R. H. Baughman and J. B. Wiley, *J. Am. Chem. Soc.*, 2001, **123**, 763.
17 K. S. Napolskii, A. Sinitskii, S. V. Grigoriev, N. A. Grigorieva, H. Eckerlebe, A. A. Eliseev, A. V. Lukashin and Y. D. Tretyakov, *Phys. B*, 2007, **397**, 23.
18 X. D. Yu, Y. J. Lee, R. Furstenberg, J. O. White and P. V. Braun, *Adv. Mater.*, 2007, **19**, 1689.
19 A. A. Grunin, N. A. Sapoletova, K. S. Napolskii, A. A. Eliseev and A. A. Fedyanin, *J. Appl. Phys.*, 2012, **111**, 07A948.
20 B. Gates and Y. N. Xia, *Adv. Mater.*, 2001, **13**, 1605.
21 A. V. Baryshev, T. Kodama, K. Nishimura, H. Uchida and M. Inoue, *J. Appl. Phys.*, 2004, **95**, 7336.
22 S. A. Grudinkin, S. F. Kaplan, N. F. Kartenko, D. A. Kurdyukov and V. G. Golubev, *J. Phys. Chem. C*, 2008, **112**, 17855.
23 T. V. Murzina, E. M. Kim, R. V. Kapra, I. V. Moshnina, O. A. Aktsipetrov, D. A. Kurdyukov, S. F. Kaplan, V. G. Golubev, M. A. Bader and G. Marowsky, *Appl. Phys. Lett.*, 2006, **88**, 022501.
24 R. C. Lecraw, D. L. Wood, J. F. Dillon Jr and J. P. Remeika, *Appl. Phys. Lett.*, 1965, **7**, 27.
25 R. Krishnan, H. Le Gall and T. K. Vien, *Phys. Status Solidi A*, 1973, **17**, K65.
26 P. Hansen and J. P. Krumme, *Thin Solid Films*, 1984, **114**, 69.
27 A. Kumar, R. C. Rai, N. J. Podraza, S. Denev, M. Ramirez, Y. H. Chu, L. W. Martin, J. Ihlefeld, T. Heeg, J. Schubert, D. G. Schlom, J. Orenstein, R. Ramesh, R. W. Collins, J. L. Musfeldt and V. Gopalan, *Appl. Phys. Lett.*, 2008, **92**, 121915.
28 M. S. Kartavtseva, O. Y. Gorbenko, A. R. Kaul, T. V. Murzina, S. A. Savinov and A. Barthelemy, *Thin Solid Films*, 2007, **515**, 6416.
29 S. E. Lofland, K. F. McDonald, C. J. Metting, E. Knoesel, M. Murakami, M. A. Aronova, S. Fujino, M. Wuttig and I. Takeuchi, *Phys. Rev. B: Condens. Matter Mater. Phys.*, 2006, **73**, 092408.
30 G. Catalan and J. F. Scott, *Adv. Mater.*, 2009, **21**, 2463.
31 M. Ristic, I. Nowik, S. Popovic, I. Felner and S. Music, *Mater. Lett.*, 2003, **57**, 2584.
32 J. Wijnhoven, L. Bechger and W. L. Vos, *Chem. Mater.*, 2001, **13**, 4486.
33 H. W. Yan, C. F. Blanford, B. T. Holland, W. H. Smyrl and A. Stein, *Chem. Mater.*, 2000, **12**, 1134.
34 J. W. Goodwin, J. Hearn, C. C. Ho and R. H. Ottewill, *Colloid Polym. Sci.*, 1974, **252**, 464.
35 P. Jiang, J. F. Bertone, K. S. Hwang and V. L. Colvin, *Chem. Mater.*, 1999, **11**, 2132.
36 S. Wong, V. Kitaev and G. A. Ozin, *J. Am. Chem. Soc.*, 2003, **125**, 15589.
37 M. P. Pechini, *US Pat.*, 3,330,697, 1967.

38 F. Marlow, Muldarisnur, P. Sharifi, R. Brinkmann and C. Mendive, *Angew. Chem., Int. Ed.*, 2009, **48**, 6212.
39 J. F. Galisteo-Lopez, E. Palacios-Lidon, E. Castillo-Martinez and C. Lopez, *Phys. Rev. B: Condens. Matter*, 2003, **68**, 115109.
40 J. Hilhorst, V. V. Abramova, A. Sinitskii, N. A. Sapoletova, K. S. Napolskii, A. A. Eliseev, D. V. Byelov, N. A. Grigoryeva, A. V. Vasilieva, W. G. Bouwman, K. Kvashnina, A. Snigirev, S. V. Grigoriev and A. V. Petukhov, *Langmuir*, 2009, **25**, 10408.
41 A. Hartsuiker and W. L. Vos, *Langmuir*, 2008, **24**, 4670.
42 S. Ghosh, S. Dasgupta, A. Sen and H. S. Maiti, *J. Am. Ceram. Soc.*, 2005, **88**, 1349.
43 S. M. Selbach, M. A. Einarsrud, T. Tybell and T. Grande, *J. Am. Ceram. Soc.*, 2007, **90**, 3430.
44 P. Vaqueiro and M. A. Lopez-Quintela, *Chem. Mater.*, 1997, **9**, 2836.
45 V. Abramova and A. Sinitskii, *Superlattices Microstruct.*, 2009, **45**, 624.
46 A. Sinitskii, V. Abramova, T. Laptinskaya and Y. D. Tretyakov, *Phys. Lett. A*, 2007, **366**, 516.
47 A. Sinitskii, V. Abramova, T. Laptinskaya and Y. Tretyakov, *Superlattices Microstruct.*, 2008, **44**, 626.
48 Y. A. Vlasov, M. Deutsch and D. J. Norris, *Appl. Phys. Lett.*, 2000, **76**, 1627.
49 M. Li, P. Zhang, J. Li, J. Zhou, A. Sinitskii, V. Abramova, S. O. Klimonsky and Y. D. Tretyakov, *Appl. Phys. B: Lasers Opt.*, 2007, **89**, 251.
50 A. Sinitskii, V. Abramova, N. Grigorieva, S. Grigoriev, A. Snigirev, D. V. Byelov and A. V. Petukhov, *Europhys. Lett.*, 2010, **89**, 14002.
51 S. G. Romanov, T. Maka, C. M. S. Torres, M. Muller, R. Zentel, D. Cassagne, J. Manzanares-Martinez and C. Jouanin, *Phys. Rev. E: Stat., Nonlinear, Soft Matter Phys.*, 2001, **63**, 056603.
52 H. M. van Driel and W. L. Vos, *Phys. Rev. B: Condens. Matter*, 2000, **62**, 9872.
53 A. V. Baryshev, A. A. Kaplyanskii, V. A. Kosobukin, K. B. Samusev, D. E. Usvyat and M. F. Limonov, *Phys. Rev. B: Condens. Matter Mater. Phys.*, 2004, **70**, 113104.
54 K. Busch and S. John, *Phys. Rev. E: Stat. Phys., Plasmas, Fluids, Relat. Interdiscip. Top.*, 1998, **58**, 3896.
55 S. G. Johnson and J. D. Joannopoulos, *Opt. Express*, 2001, **8**, 173.